

## Forensic Engineering Analysis of Electro-Shock Weapon Safety

by James Angelo Ruggieri, P.E. (NAFE 601M)

### Abstract

Electro-shock weapons have become increasingly popular with law enforcement agencies in recent years as alternatives to firearms. In particular, the Taser® brand of electro-shock weapons are characterized by a distinctive product feature that propels electrode barbs at the subject – allowing the officer to exert control over the subject while maintaining some safe distance. These model weapons offers two modes of operation: the projectile or ballistic mode, where the electrode barbs can reach out to the subject at a 15-foot or greater distance, and a backup, touch or drive stun mode, that requires the officer to “drive” the weapon into the subject. This latter mode of operation is an alternative mode of operation should the electrode barbs miss the subject, or for use in close quarters situations.

The manufacturer of these weapons, Taser International Inc., claims the devices to be safe, citing many independent technical and medical safety studies. However, following over one hundred deaths involving use of the weapon, the company has received much criticism, and consequently, named as a defendant in a large number of lawsuits under theories of defective product, wrongful death, and willful misrepresentation of product performance and product safety.

This paper reports the findings of independent electrical tests performed on a civilian model version, the 18-Watt Taser (Model M18.) The Taser M18 model is identical to the 26-Watt M26 model police version involved in many of these death/injury cases, with the exception that the M26 produces more pulses per second than the M18, and thus (8) eight Watts more power.<sup>1</sup> The independent test findings disclose that the product produces considerably more power and current than claimed by the manufacturer when tested to model drive-stun contact with realistic load resistance values characteristic of human tissue. In the drive-stun mode of operation, the test results show the weapon supplies at least 6.6 Amperes<sub>RMS</sub> (or about 50 times more current than the manufacturer's published current rating of 133 mA<sub>RMS</sub>) in human tissue at 2.2 kV peak-to-peak\* at a pulse repetition rate of 14 pulses per second. When tested using realistic

\* Output voltage of the weapon decreases with decreasing load resistance, and the manufacturer's 50 kV output rating ostensibly relates to the weapon's no-load condition, or the voltage supplied by the weapon to bridge the spark gap between the two electrodes.

human tissue resistance values, the output waveform quickly degenerates from a damped sinusoidal waveform to negative monophasic impulses having a waveform epoch interval of 2  $\mu$ s with a fundamental frequency of 500 Hertz. The findings show the energy delivered by the weapon to be considerably understated by the manufacturer when contrasted to the provisions of key commercial-consensus industry standards governing electrical shock safety. In this regard these findings place the weapon well into the "lethal"† category. The weapon is determined to be most lethal when used in the drive-stun mode of operation because of certain inherent system losses present in the ballistic mode not present in the drive-stun mode, and because the energy supplied by the weapon is not regulated through either active or passive circuitry.

Although this paper focuses on actual conditions for the drive-stun mode of deployment, an evaluation is also made of the applicable modeling considerations of the weapon in the ballistic mode as a means of contrasting relative lethality to the drive-stun mode, as well as to identify deficiencies in manufacturer's claims. It is beyond the scope of this paper to assess the internal workings and circuitry of the device; rather, this paper treats the weapon as a simple *black-box* entity and focuses on the ultimate energy delivered by the weapon given human physiology electrical factors.

### 1.0 Taser M18

The Taser M18 is a hand-held electronic stun gun which fires two tethered electrically conductive barbed darts. The fishhook-like darts are designed to penetrate the skin and deliver high-voltage electrical pulses through thin, flexible electrical conductors. According to the M18 product's operating manual<sup>2</sup> and Taser commissioned studies<sup>3</sup>, the Taser model M18 delivers 18 Watts of power using a train of 11  $\mu$ s pulses at a rate of 10-pulses per second. The manufacturer claims that each pulse produces 50 kV at 1.76 Joules per pulse, supplying a current of 133 *m*.A RMS.

### 2.0 Computations and Measurements and Nomenclature

The Taser Model M18 weapon is a hand-held spark-discharge weapon that integrates two electrode contacts, approximately 2.40 mm by 3.4 mm<sup>†</sup> (i.e., 8.1 mm<sup>2</sup> surface contact area) at the face of the weapon and intended for direct electrical connection with a human subject (Figure No. 3). The manufacturer defines the mode of operation where the integral electrodes are directly applied to a human subject as the "drive-stun" mode, in contrast to the weapon's remote or

† Lethal - 1a: of, relating to, or causing death <death by lethal injection> b: capable of causing death <lethal chemicals> 2: gravely damaging or destructive. Merriam-Webster's Collegiate Dictionary, 11th Edition.

‡ Approximately the size of a match head.

"ballistic" mode of operation using tethered, electrically conductive, fishhook-like projectiles (Figure No. 4). The integral electrode contacts are directly connected to the secondary terminals of an internal step-up transformer having a measured secondary resistance of approximately 77.5 ohms, defining a *floating* system since there is no ground reference (Figure No. 5).

When the projectile mode is desired, the integral electrode contacts at the face of the weapon are also used to electrically connect and interface with an expendable air-cartridge assembly (Figure Nos. 1 & 2). The air-cartridge assembly houses two projectile barbed probes, two 17-foot coils of thin gauge insulated wire, a pressurized Nitrogen propellant source, two *fly-away* "blast" doors, and two additional extended drive-stun electrodes that can facilitate drive-stun operation while the air cartridge is in place<sup>§</sup> (Figure Nos. 1 & 2).

When high voltage is applied across a gap occupied by a gas, the gas is ionized through an avalanche effect that forms a conducting plasma channel. However, plasma is not an ideal conductor, but the resulting heat by-product caused by the large current flow across the air gap serves to maintain ionization and conduction. Conduction continues until the gap potential difference (and/or drop in heat) drops to the shut-off level.<sup>4</sup> Spark gaps are frequently used in high-voltage over-voltage protection schemes to serve as electrical pressure-relief valves — clamping system voltage because the large current flow creates substantive voltage drops across the gaps. Therefore, the power losses occurring in systems using spark gaps can be modeled and represented as series-resistive elements in equivalent circuit models.<sup>5, 6, 7, 8</sup>

In the projectile mode of operation, the M18 exhibits three pairs (i.e., six spark gaps) between the weapon's integral contacts and the barbed projectiles. These spark gaps are represented as resistors in Figure No. 5 — showing the estimated resistance of the spark gaps during conduction. The diagram also notes the contributory resistance introduced by the two conductors feeding the projectile barbs. Such spark gap losses are present only when the weapon is used in the ballistic mode and not when the weapon is used in the drive stun mode with integral contacts. Because these resistive elements (system losses) are not present in the drive-stun mode of operation, the Taser weapon delivers *more* power in the drive-stun mode than in the projectile mode.

To avoid the ambiguity caused by inconsistent usage among industry for the many "deprecated synonyms" governing pulses,<sup>9</sup> the term *Power Contributing*

1211

§ The intention of the extended drive-stun electrodes is to provide the user an alternate drive-stun means while the air-cartridge is in place in the event of failure of the barbed projectiles (e.g., the barbs miss the subject, or a projectile discharge failure, etc.) or for use in close quarter circumstances.

*Interval (PCI)* is used herein to describe the results of the tests. The PCI is defined to be the *waveform epoch* \*\*, or the resulting waveform time interval from the trigger point (i.e., zero) up to the point where the curve returns back to a steady-state zero. The PCI may include multiple pulse cycles. For instance, in Figure Nos. 13, 14, and 15, the PCI is 70  $\mu$ s while the pulse cycle is only 20  $\mu$ s (i.e., three zero crossings or the pulse period), and the pulse width is the time interval between the 10% and 90% amplitude values of the pulse cycle (i.e., 18  $\mu$ s)††. The 70  $\mu$ s PCI shown in Figure Nos. 13, 14, and 15 covers approximately three and one-half pulse cycles.

### 3.0 Testing Procedure

Testing and analysis were performed in accordance with established industry standards, guidance, and nomenclature.<sup>10, 11, 12, 13, 14, 15, 16</sup> It is important to note that the output of the Taser M18 weapon is a *floating* system in that there is no reference to ground. In all the tests described in this paper, the weapon was instrumented differentially using two channels of a Tektronix TDS 3012B digital phosphor oscilloscope and two Tektronix P6015A high-voltage probes.<sup>17</sup> The oscilloscope provides a differential math control feature to permit the subtraction of Channel B from Channel A - facilitating truer measurement and analysis of the output waveform. Differential testing improves the accuracy of high-voltage measurements, particularly fast-rise time signals since common mode voltage, such as noise introduced by ground loops, is cancelled.<sup>17, 18</sup> The ideal differential measurement system responds only to the potential difference between two terminals. The differential voltage across the circuit pair is the desired signal, yet an unwanted signal can exist that is common to both sides of a differential circuit pair.<sup>19</sup> The unwanted voltage is known as common-mode voltage. The differential measurement system rejects, rather than measures common-mode voltage, and therefore improves measurement accuracy and precision.<sup>20</sup> The test fixture and connections used in these tests are described in Figure No. 6.

The oscilloscope also captures and stores waveform data and supplies a record of the measurements in a spreadsheet-compatible format. This record provides waveform time and amplitude data, which was exported into a spreadsheet and other math-handling applications for further processing.

\*\* IEC 60469-1 (Reference No. 13 et al), definition 2.3.2.

†† In a pulse waveform, the interval between (a) the time, during the first transition, that the pulse amplitude reaches a specified fraction (level) of its final amplitude, and (b) the time the pulse amplitude drops, on the last transition, to the same level. Note: The interval between the 50% points of the final amplitude is usually used to determine or define pulse duration, and this is understood to be the case unless otherwise specified. Other fractions of the final amplitude, e.g., 90% or 1/2 may also be used, as may the root-mean-square (rms) value of the pulse amplitude. (IEEE 100-1996)

‡‡ NIST Certificates of Traceable Calibration valid for probes, oscilloscope, and DMM used in all the tests described herein.

The methodology used in performing power and current computations of the captured pulse waveform and data effectively integrates and evaluates the area under the pulse waveform curves. In each experiment, the captured waveform was segmented to the maximum resolution capability of the test instrument, and evaluation of the waveform content was limited to the duration of the power-contributing interval. Resolution, record length, waveform epoch or PCI, peak-to-peak voltage,  $I_{RMS}$ , Joules per pulse and Watt-second data accompany the processed waveform recordings provided in this paper (Figure Nos. 9, 12, 15, 18, and 21).

### 4.0 Computations

Power computations for each waveform segment were performed as follows:

$$\text{Joules per segment} = \frac{V^2}{R} * I_T \quad \text{Equation 1}^{21}$$

Where:

$V$  = Peak waveform voltage, Volts

$R$  = Load Resistance, Ohms

$I_T$  = Interval Time, Seconds

Joules per PCI is computed as the sum of all segmented power values, or

$$\text{Joules/PCI} = \sum_{i=1}^n \frac{V_i^2}{R} * I_T \quad \text{Equation 2}^{22}$$

Where:

$n$  = number of segment intervals

Watts per second or total Joules is simply the number of PCIs per second times Joules per PCI, or:

$$\text{Watt Seconds (Joules)} = \text{PCI} / s * \sum_{i=1}^n \frac{V_i^2}{R} * I_T \quad \text{Equation 3}^{23}$$

Current  $I_{RMS}$  is computed as:

$$I_{RMS} = \sqrt{\frac{P}{R}} \quad \text{Equation 4}^{24}$$

where:

$I_{RMS}$  = root-mean-square current in Amperes

$P$  = power in Watt-Seconds, or Joules

$R$  = load resistance in Ohms

Except for the aforementioned waveform dissection method for determining Joules per pulse, the computations performed herein are identical to the computation methods performed by Harrison of Carleton University for Taser International, Inc. Although Harrison describes the general integral formula in his report, the polynomial describing the curve is not identified. Reportedly, Harrison never actually instrumented the weapon to determine the power-contributing interval, and instead relied upon data supplied by Taser International.

### 5.0 Power Source

New, current date-code batteries were used for each resistance load test experiment, including probe error tests that preceded each of the experiments. The weapon uses eight (8) AA, Alkaline 1.5 Volt batteries configured in a removable battery pack for a nominal series voltage of 12 V. For all tests identified in this paper, Duracell brand, Ultra batteries were exclusively used and is one of the three battery types recommended by the manufacturer. Taser International also recommends Energizer  $\epsilon^2$  and Energizer NH-15 NiMH rechargeable batteries.

Newly configured battery pack terminal voltages exhibited minimal variation when measured immediately prior to the experiments:  $12.935 \text{ V} \pm 1.85\%$  unloaded. However, tests performed to determine battery depletion rate disclosed that battery pack terminal voltages decreased substantively following four (4) successive firings (5-second cycles) spaced 5 minutes apart to permit cooling of the weapon's internal components and batteries. Following four unloaded firings in the drive-stun mode, battery pack terminal voltage dropped about 11% to an average value of 11.5 V while the pulse rate dropped about 7% from over 14 PCIs per second to just over 13 PCIs per second.

### 6.0 Load Resistors and Human Tissue Resistance Modeling

Zero-inductance 10-Watt, high-voltage carbon composition resistors were used as test loads. The resistors were configured in various series-parallel arrays to provide measured values of 1100.00, 128.05, 55.02, 32.29, and 16.14 Ohms  $\pm 1\%$ . Resistor lead and instrument connection inductances were minimized by careful arrangement of the devices and equipment to minimize test lead length to the device under test. Load resistor values used in the tests were selected to model human tissue resistance values at high voltage. The electrical output for the Taser weapon is a function of the loading on the Taser weapon,<sup>24</sup> and with decreasing load resistance, current increases as described by the  $I=E/R$  relationship. The internal impedance of the human body is considered mostly resistive and skin impedance becomes negligible, when the skin breaks down or when tissue is exposed to high touch voltages.

A note in the referenced IEC document states:

"Above 1000 V, it may be assumed that the influence of the skin impedance is negligible, and therefore,  $Z_T$  and  $R_T$  have practically the same value" IEC 479-1, Annex C, page 61.

This means that at voltages above 1000 Volts, the total impedance,  $Z_T$  is equal to the total resistance,  $R_T$ , and reactance may be neglected without impairing accuracy.

Because the tested output voltage of the device in the drive-stun mode is  $2 \text{ kV} < 25 \text{ kV}$  (range of voltages when loaded with the resistor values identified herein) we simplify assumptions and analysis of the test models by neglecting reactance and using published values for total internal resistance as specified in IEC 479-1. For the range of touch voltages measured in the subject weapon ( $2 \text{ kV} \leq 25 \text{ kV}$ ) total body resistance hand-to-hand for 95% of the population is approximately 850 Ohms.<sup>25</sup> Tables 2 and Figure 4 of the IEC 479-1 standard shows the total body impedance for living human beings for the current path hand-to-hand, or hand-to-foot to asymptote to 850 Ohms, at about 5kV for 95% of the population.

However, the values given in the IEC479-1 table 1 are based on a "large" electrode cylindrical contact surface area of  $8,000 \text{ mm}^2$ <sup>27</sup> and the measured surface area of the integral electrodes of the Taser weapon is only  $8,125 \text{ mm}^2$  (See discussion in Figure No. 3) — about 985 times smaller than the  $8,000 \text{ mm}^2$  area identified in IEC 479-1 Table 1. IEC 479-1 Figure 10, Curve D (i.e., 10  $\text{mm}^2$ ) describes the total body impedance, hand-to-hand, or hand-to-foot for the weapon's  $8,125 \text{ mm}^2$  integral contacts to be about 35K Ohms. The resistance value for the distance between the heart and pelvic girdle ( $\sim 305 \text{ mm}$ ) is  $1.3\%$  of the hand-to-hand value,<sup>28</sup> or in this case,  $35\text{K Ohms} \times 0.013 = 455 \text{ Ohms}$ . However, the distance between the integral contacts of the weapon is 37mm, or about 1/8 the heart to waistline distance of 305 mm. Assuming homogeneity of human tissue between the heart and pelvic girdle, we compute  $455 \text{ Ohms} / 0.1213 = 55.2 \text{ Ohms}$  for the predicted resistance of human tissue given the 37 mm (drive-stun mode) spacing between subject electrodes with a electrical contact surface area of  $8,125 \text{ mm}^2$ . Therefore, the initial predicted load resistance presented to the weapon in the drive-stun mode is 55 Ohms and this resistance will drop significantly and quickly with the duration of current flow because of resulting tissue damage<sup>29</sup> and electroportation.<sup>30</sup>

§§ Cylinder 100mm long by 80mm diameter — about the size of a coffee mug.

The resistance of damaged tissue drops because of swelling that increases surface contact area between the electrodes and tissue. This creates a runaway effect of increasing current with decreasing resistance. In addition, Joule heating increases tissue temperature, resulting in decreasing tissue resistivity,<sup>31</sup> eventually falling to zero when charred.<sup>32</sup>

Electroporation is yet another phenomena that serves to impact tissue resistance. The effects of high voltage pulses on human skin have been studied in evaluating transdermal drug delivery systems.<sup>33</sup> High voltage pulses create aqueous pathways that increase skin permeability to ions and macromolecules, allowing drugs to more easily pass through the skin and into the body. Tests performed by Gowrishankar<sup>34</sup> found human tissue resistance to decrease by as much as three orders of magnitude in response to high voltage pulses ( $U_{skin} > 150V$ ,  $T_{pulse} = 1$  ms). In one experiment using 500 V one-millisecond pulses, Gowrishankar showed skin resistance to decrease by a factor of nearly one hundred following only a few pulses. Gowrishankar applied the pulses once every five seconds across full-thickness human cadaver skin and measured the impedance between pulses, causing a starting impedance of  $200K\Omega$ <sup>\*\*\*</sup> to rapidly drop to less than  $3.8 K \Omega$  within the first ten pulses, and thereafter settle to a steady-state value of  $2.1K \Omega$  over the next few pulses. At the end of the pulsing, the skin impedance recovered by 200-400  $\Omega$  within the first minute, but reached only  $3K \Omega$  in the next hour. This shows tissue resistance behavior to high voltage pulses to be dynamic and not static, and output energy computations for pulsing stun-gun devices on human tissue must consider the initial (pre-pulse) tissue resistance and the rapidly declining resistance. Gundersen et al and Schoenbach et al show that to avoid cell membrane damage caused by electroporation, yet still affect the intracellular structure, pulses must be much shorter ( $\mu S$  and sub  $\mu S$ ) than  $1 \mu S$ .<sup>35, 36</sup>

Applying Gowrishankar's findings to the corrected initial tissue resistance of 55 Ohms computed for the Taser model M18 37-mm spaced electrodes, we compute the resistance tissue resistance to be:  $55/100 = 0.55$  Ohms within approximately 20-pulses. Given the slow tissue resistance recovery rate observed by Gowrishankar, the *new initial* resistance seen by the weapon in a subsequent pulse burst application within minute of the first burst would be about the same value of about 0.55 Ohms.

### 7.0 Frequency and Pulse Width

Human tissue sees 60 Hz current as one-hundred-twenty 8.3 millisecond alternating polarity (biphasic) pulses per second. Reilly concludes the current rever-

sal of a biphasic waveform can reverse the development of membrane excitation caused by the initial phase of the stimulus and thus elevate excitation thresholds<sup>37</sup> - suggesting that biphasic waveforms may pose less of a risk than monophasic waveforms. Reilly also determined experimentally that the perception thresholds for cardiac tissue were reduced an average of 23% for negative monophasic pulses compared with positive polarity pulses.<sup>38</sup>

Koscove notes lack of any experimental data on the clinical effects on ventricular fibrillation (VF) with a train of damped sinusoidal waves as a function of pulse frequency, pulse duration, amplitude, current and frequency.<sup>39</sup> Equally, IEC 479-2 does not associate frequency and VF risk for frequency values above 1kHz. For frequencies falling between 1 kHz and 10 kHz, the issue is presently under consideration<sup>40</sup> by the IEC TC 64 working group, however nothing tangible has yet been developed, while for frequencies above 10 kHz, the working group indicates lack of any experimental data to help predict VF risk.<sup>41</sup>

However, Geddes states that assumptions that only low-frequency alternating current can induce ventricular fibrillation are *invalid*, and shows that a single pulse of current applied to the body, as well as high frequency current, to induce ventricular fibrillation.<sup>42</sup> Geddes reports occurrences of ventricular fibrillation following application of electro-surgical current with a frequency in the megahertz range<sup>43</sup>, and identifies shock hazards from transients in SF<sub>6</sub> insulated, coaxial, high-voltage power cables consisting of two damped sinusoidal components: one at 7 MHz and the other at 0.29 MHz.<sup>44</sup>

With respect to current penetration in tissue as related to frequency, this author previously demonstrated that Skin Effect phenomenon, as related to the Taser weapons, is an unsound claim since scientific evidence shows that skin depth phenomenon becomes a significant consideration only when frequency is well above 10 MHz.<sup>45</sup> Similarly, Reilly shows that with increasing frequency,  $I^2R$  energy tends to dissipate in deeper tissue than flow at the tissue/electrode surfaces.<sup>46</sup>

\*\*\*  $\Pi$  mm<sup>2</sup> surface area of electrodes

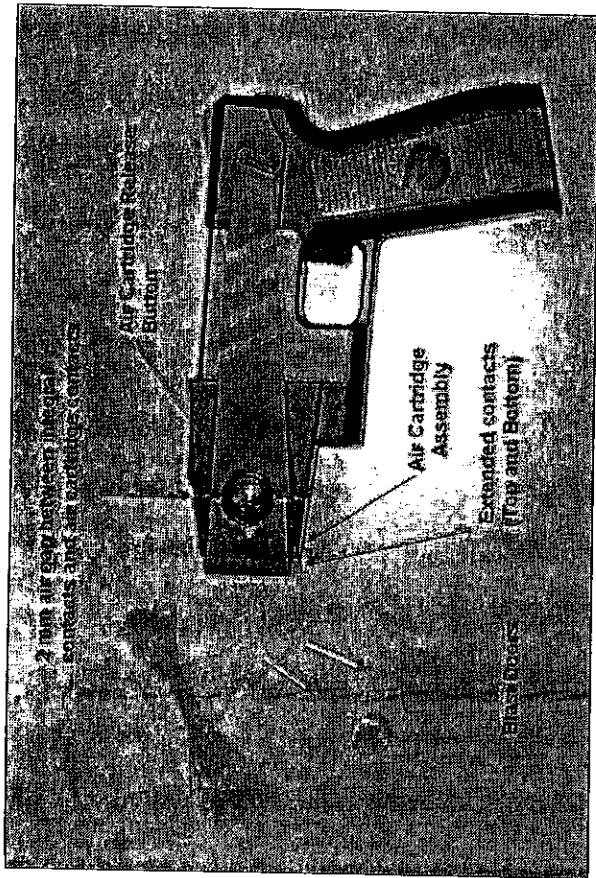


Figure 1

Taser Model M18 side profile shown with attached, expended air-cartridge

The figure shows (two) coiled conductors; each about 5.15 meters long (17 feet), attached electrode bars (shank: 9 mm long by 0.78 mm diameter), and plastic flyaway blast doors. A 2-mm air gap couples the integral contacts located at the face (muzzle view) of the weapon and the air cartridge circuitry. In the ballistic mode of operation, arcing can be observed occurring between the integral contacts at the face of the weapon and the receiving contacts at the rear of the air cartridge - serving to energize the conductors and attached electrode projectiles and the two extended electrodes located at the face of the air cartridge. The conductors are made from a single solid strand, coated steel-alloy, with an overall plastic insulation. The conductor diameter is 0.11 mm (0.0043-inches or 4.33 mils: ~37 AWG) and the overall OD of the conductor is 0.45 mm. Measured resistance of the 5.15 length of conductor is 17.9 ohms, or about 3.48 ohms/meter. The projectile barb assemblies are not directly connected to the conductor in the conventional sense, instead, the conductor terminates at the rear of the barb ferrule with a strain-relieving knot - relying on the high-voltage produced by the weapon to breakdown the insulation to make an electrical connection with the projectile ferrule and barbed tips. This connection method is also used at the air cartridge end, such that a conventional ohmmeter will read an "open" condition when the barb and the receiving tab of the air cartridge are instrumented. Overall, this connection scheme presents several resistance obstacles, or losses, when the weapon is used in the projectile mode, and therefore, facilitates the expectation that the weapon will deliver less energy to the subject when used in this latter manner. However, such obstacles are not present when the device is used in the drive-stun mode without an air cartridge (via the integral contacts). Figure No. 4 shows the "knot" termination method used connect the conductors with the barb ferrule projectile and Figure No. 5 describes the physical and equivalent models.

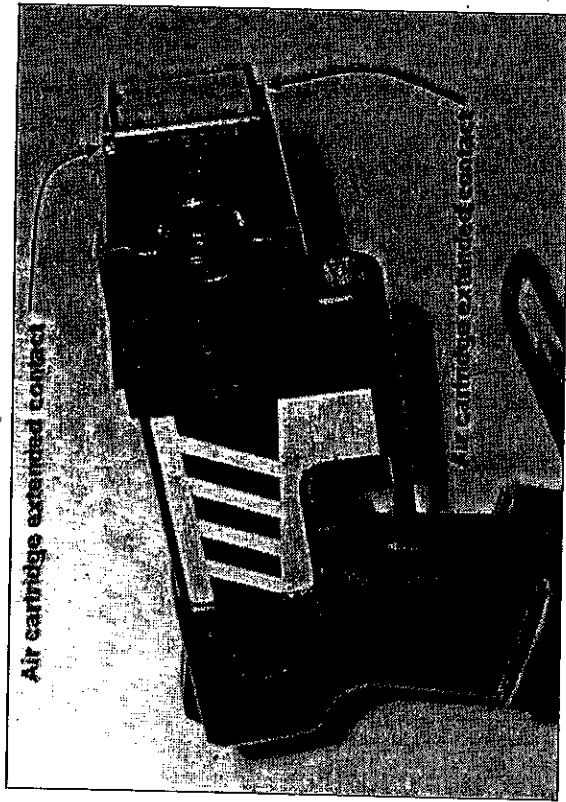
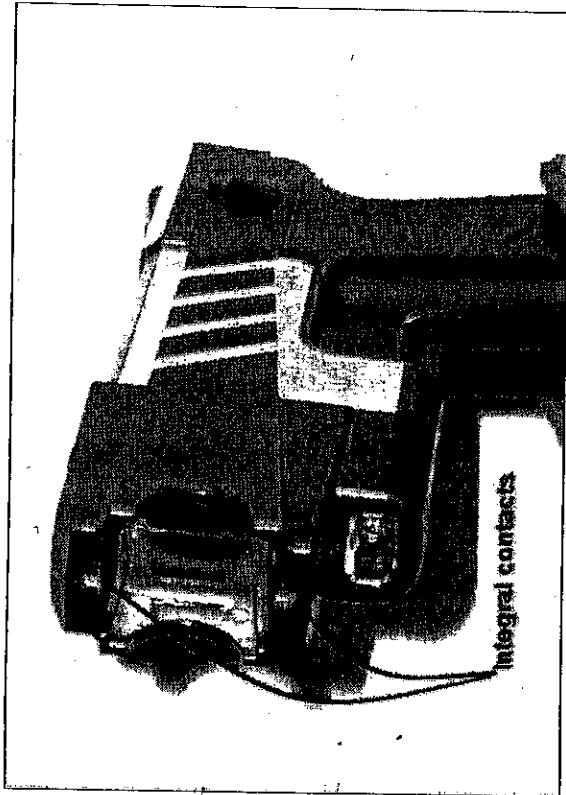


Figure 2

Taser Model M18 skewed perspective shown with attached, intact air-cartridge

The figure shows an intact air cartridge (ready to fire) and the extended contacts at the face of the air cartridge (top and bottom). The extended contacts are recessed approximately 3 mm back from the face of the air cartridge, and during the drive-stun operating mode with the weapon orthogonal to a plane of the target, arcing can be observed between the extended contacts and the target. Because the contacts are recessed from the face of the weapon, arcing between the contacts and the subject occurs, and thus an increased likelihood for greater burn damage than with the higher profile integral contacts.



**Figure 3**  
Taser Model M18 skewed frontal perspective without air-cartridge showing the two integral contact points.

The figure shows the integral contacts at the face of the weapon. In this state, the weapon is used to drive-stun the subject. The integral contacts extend about 2.5 mm from the face of the weapon, and when pressed upon the subject's body, provide positive electrical coupling between the weapon and the subject. The contacts are spaced about 37 mm on centers. In this mode of operation, there is no arcing between the subject and the electrical contacts of the weapon, and thus no source of energy loss. In this mode of operation, the weapon delivers its maximum power capability.

The dimensions of each integral contact are 2.50 mm by 3.25 mm, providing a per contact surface area of 8.125 mm<sup>2</sup>. At the manufacturer's published current output of 133 mA, current density equals 16.37 mA/mm<sup>2</sup> - associated only with skin reddening (Zone 1),<sup>47</sup> however, 2nd degree burns and blisters as well as carbonization of the skin are frequently observed following application of the weapon in this mode - equating more closely with IEC Zone 2 and Zone 3 type damage. Mapping the observed damage to the range of current densities for IEC Zone 2 (20 mA/mm<sup>2</sup> to 50 mA/mm<sup>2</sup>) and IEC Zone 3 (>50 mA/mm<sup>2</sup>) suggests more current supplied than published by the manufacturer. Working backwards from the frequently observed tissue damage, and given the measured contact surface area of 8.125 mm<sup>2</sup>, we compute output current supplied to surpass 133 mA and possibly exceed 406 mA (e.g., Zone 3 skin carbonization type damage).

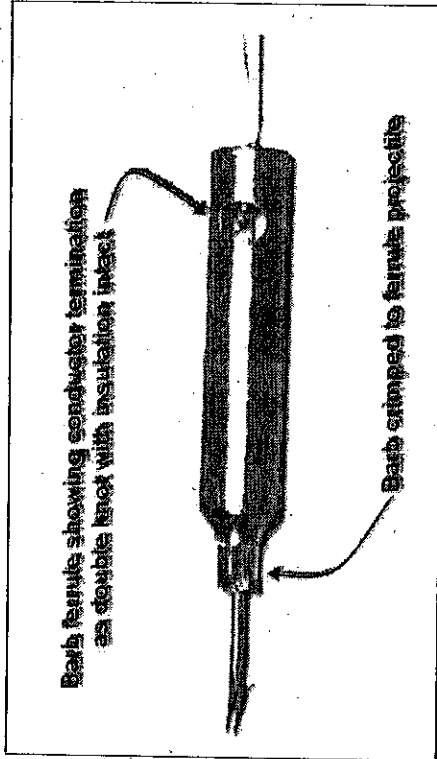


**Figure 4**  
One of two barbed projectiles and tethered conductor

The metallic harpoon-like barb and shank is crimped in the brass ferrule projectile, while a double knot securely fastens the electrical conductor to the projectile. The knotted arrangement can be seen in the ferrule's transverse opening. The conductor's insulation is intact, and the method of conveying the charge from the conductor to the barb assembly relies on the high-voltage (e.g., 50 kV) emanating from the weapon to break down the insulation to couple with the conducting projectile. Electrical contact surface area of each barb/shank:  $2\pi r * length = 2.45 \text{ mm} * 9 \text{ mm} = 22.05 \text{ mm}^2$

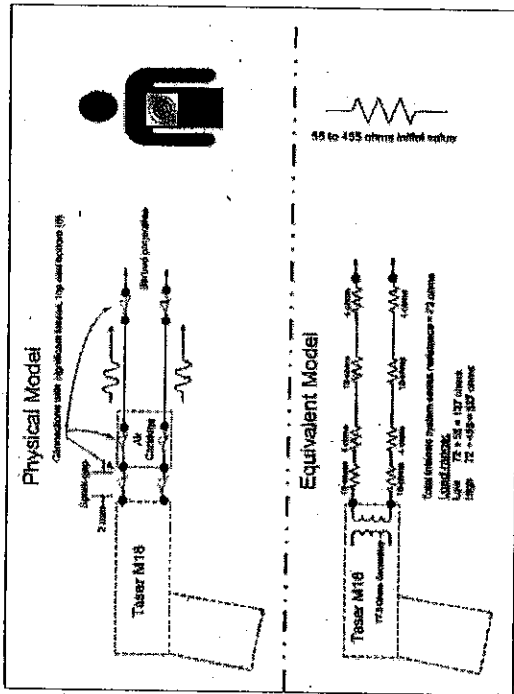


Figure 5  
Physical Model and Corresponding Electrical Equivalent Model of the Taser M18.

The models show the points of losses when the weapon is used in the ballistic mode versus the drive-stun mode. Arc-conducting resistances are shown in the equivalent model. In the drive-stun mode of operation, there are no external system losses since the output of the weapon is in direct contact with the subject (load) and it is in this mode of operation that the weapon supplies its maximum capable energy to the subject. Depending on electrode-barb spread (a function of firing distance between weapon and the subject), the initial electrical resistance loading from a hit on the torso can vary from about 455 Ohms for a full torso spread from top of chest to waistline, to about 55 Ohms for a 37 mm spacing between electrodes. (See discussions in paragraph 6.0 herein). The maximum power transfer from source to load occurs when the source impedance equals the complex conjugate of the load impedance, or  $R_S + jX_S = R_L - jX_L$ . When this relation is satisfied, the energy transferred from the source to the load is maximized.<sup>48</sup> Since the human tissue reactance is insignificant for the high voltages present, we can neglect reactance for both the load and the source to arrive at a rough approximation for maximum transfer efficiency. In theory, this occurs when the total load system is 77.5 Ohms. For the drive stun mode with integral contacts, this means the tissue load should be at 77.5 Ohms, and in the projectile mode, tissue resistance should be at 5.5 Ohms (*total intrinsic system series resistance + tissue resistance = 72 Ohms + 5.5 Ohms = 77.5 Ohms.*)

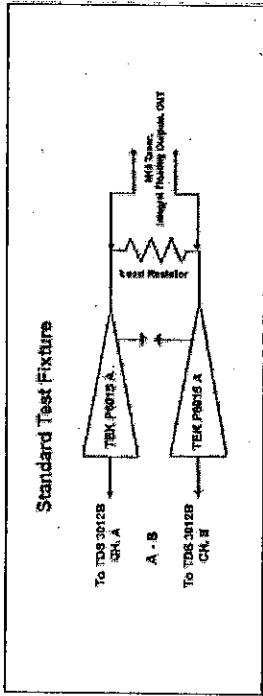
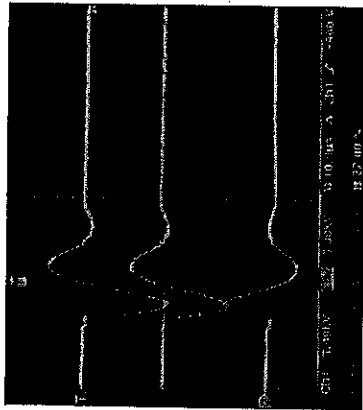


Figure 6  
Test Equipment Configuration - Standard Test Fixture

Test instrumentation configuration is straightforward: two (2) Tektronix High-Voltage Probes, Model No. P 6015A, feed two independent channels of a Tektronix TDS 3012B Digital Phosphor Oscilloscope. Trigger is taken from channel A input. Oscilloscope waveform math is performed to subtract one channel from the other (i.e., A-B, or differentially) as a means of minimizing measurement error owed to common mode noise. Amplitude and frequency response skew tests were performed prior to testing at each load resistance as a means of characterizing error introduced into the system by the two probes. In every test case, the probes were shown to be matched (i.e., traces overlap perfectly) and compensation was not required, and uncertainty introduced by differences between the two probes is considered negligible. Measurement uncertainty is the aggregate sum of all equipment errors: +/- 10%. Sources of errors are the two probes, oscilloscope, and the analysis-dependent measurements of other equipment (i.e., DMM to proof resistance values, etc).



**Figure 7**  
Triple Trace, 1100 Ohm Loading.

Three-trace screen capture. Channel 1 in yellow (top), Channel 2 in blue (bottom) and resulting differential, red trace (CH1 - C2) in middle. Vertical scale settings for channels 1 & 2 are 5 kV per division and 10 kV per division for differential trace. Horizontal time scale setting is 10  $\mu$ S per division. Peak-to-Peak voltage is 29.5 kV

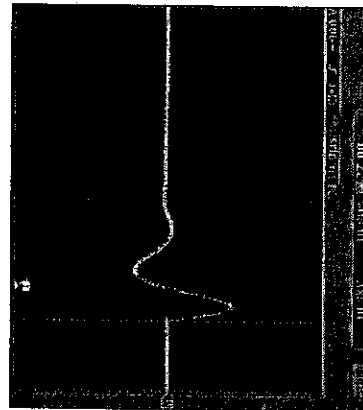


**Figure 8**

Differential Trace at 1100-Ohm Load.

Math trace of Figure 7. Vertical cursors define power contributing pulse interval. At 10  $\mu$ S/division time scale, power contributing area of interest resides between two vertical measurement cursors to trap a 32  $\mu$ S PCI.

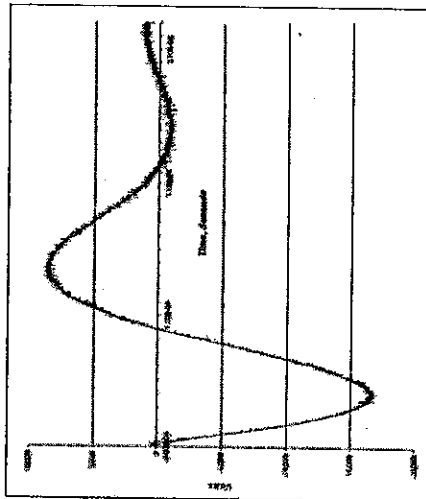


**Figure 9**  
1100 Ohm Loading, 32  $\mu$ S PCI.

Waveform analysis of recorded instrument data.

Data Points:	3,201
Resolution:	10E-9 sec.
PCI:	32 $\mu$ S
Peak-to-Peak Voltage:	29.5 kV
Joules per Pulse:	1.41
Pulses per Second:	14
Watts:	19.76
I <sub>RMS</sub> :	134 mA
Frequency:	50 kHz

At an 1100-Ohm test load, we can see that the weapon's output current is consistent with manufacturer's rating of 133 mA. However, as discussed in paragraph 6.0 herein, 1100 Ohms exceeds the highest possible human tissue resistance of 850 Ohms (hand to foot). Moreover, placement and connection of weapon's electrodes in a hand to foot scenario is impossible, even in the projectile mode. The PCI is about 32  $\mu$ S and not 11  $\mu$ S as claimed by the manufacturer. The resistance value used by the manufacturer in computing and relating energy output of the weapon, 1000 Ohms, is incorrect and does not represent realistic human tissue resistance values. As shown in the forthcoming graphs, as the resistance is reduced to model actual loading, the current increases significantly.

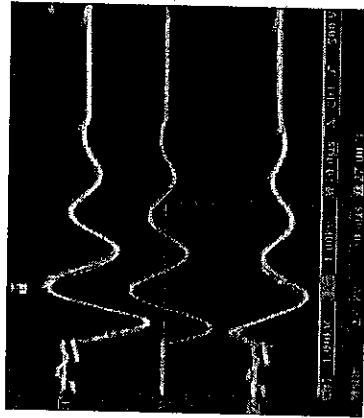


**Figure 10**

Triple Trace, 128.05 Ohm Loading.

Three-trace screen capture. Channel 1 in yellow (top), Channel 2 in blue (bottom) and resulting differential, red trace (CH1 - C2) in middle. Vertical scale settings for channels 1 & 2 are 5 kV per division and 10 kV per division for differential trace. Horizontal time scale setting is 10  $\mu$ S per division. Peak-to-Peak voltage is 4.40 kV. Some instability in the weapon output appears as common mode noise on the Channel 1 and Channel 2 traces; however, ultimately cancels out in the resulting differential red center trace.

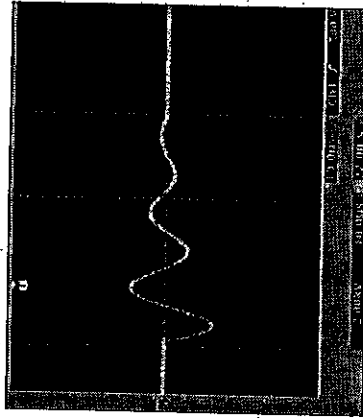


**Figure 11**

Differential Trace at 128.05-Ohm Load.

Math trace of Figure 10. Vertical cursors define power-contributing interval. At 10  $\mu$ S/division time scale, power contributing interval of interest resides between two vertical measurement cursors to trap a 60.0  $\mu$ S waveform. Contrasting Figure 8 to Figure 11 shows a pattern that holds throughout: increasing PCI with decreasing load resistance.

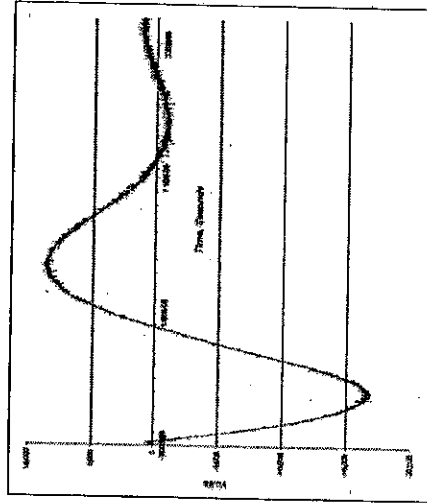


**Figure 12**  
128.05 Ohm Loading, 60  $\mu$ S PCI.

Waveform analysis of recorded instrument data

Data Points:	6,020
Resolution:	1E-8 sec.
PCI:	60 $\mu$ S
Peak-to-Peak Voltage:	4.4 kV
Joules per Pulse:	0.416
Pulses per Second:	14
Watts:	5.825
I <sub>RMS</sub> :	213 mA
Frequency:	50 kHz

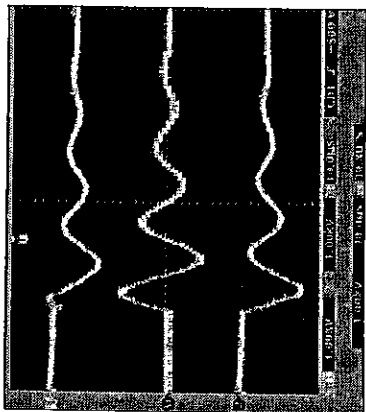


Figure 13

Triple Trace, 55.02 Ohm Loading.

Three-trace screen capture. Channel 1 in yellow (top), Channel 2 in blue (bottom) and resulting differential, red trace (CH1 - C2) in middle. Vertical scale settings for channels 1 & 2 are 1 kV per division and 1 kV per division for differential trace. Horizontal time scale setting is 10  $\mu$ S per division. Peak-to-Peak voltage is 2.2 kV.

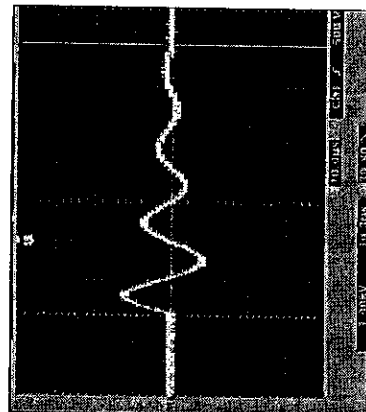


Figure 14

Differential Trace at 55.02-Ohm Load.

Math trace of Figure 13. Vertical cursors define PCI. At 10  $\mu$ S/division time scale, power contributing interval of interest resides between two vertical measurement cursors to trap a 70  $\mu$ S waveform epoch

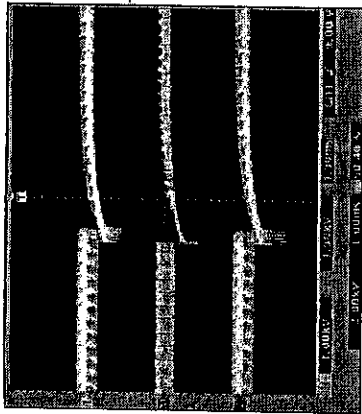


Figure 16

Triple Trace, 32.29 Ohm Loading.

Three-trace screen capture. Channel 1 in yellow (top), Channel 2 in blue (bottom) and resulting differential, red trace (CH1 - C2) in middle. Vertical scale settings for channels 1 & 2 are 1 kV per division and 2 kV per division for the differential trace. Horizontal time scale setting is 1 mS per division. Peak-to-Peak voltage is 2.20 kV. The output is no longer a damped sinusoidal waveform, but a negative monophasic impulse with a 2 mS PCI.

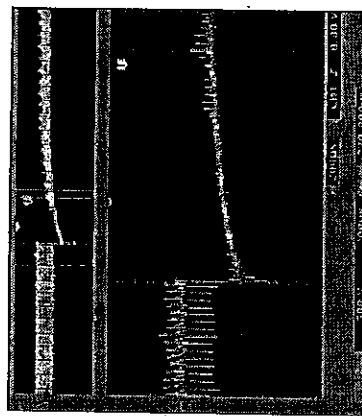


Figure 17

Differential Trace at 32.29 Ohm Load. Waveform expansion.

Math trace of Figure 16. Vertical cursors define power contributing pulse interval. At 200  $\mu$ S/division time scale, vertical measurement cursors trap a 1.20 mS segment of the 2 mS PCI

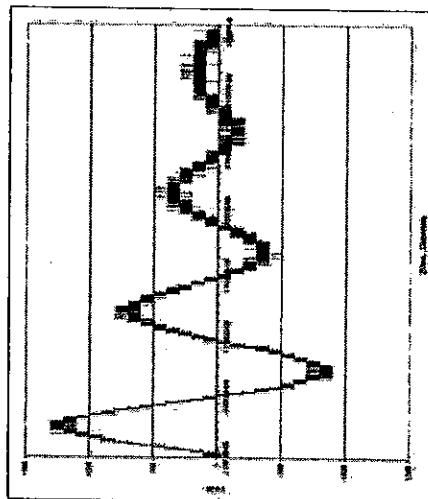


Figure 15

55.02 Ohm Loading, 70  $\mu$ S PCI.

Waveform analysis of recorded instrument data

Data Points: 7,001  
 Resolution: 1E-8 sec.  
 PCI: 70  $\mu$ S  
 Peak-to-Peak Voltage: 2.2 kV  
 Joules per Pulse: 0.2546  
 Pulses per Second: 14  
 Watts: 3.565  
 I<sub>RMS</sub>: 254 mA  
 Frequency: 50 kHz

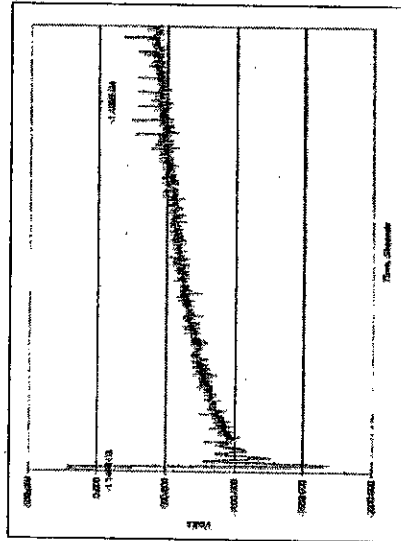


Figure 18

32.29 Ohm Loading, 2.00 mS PCI†††

Waveform analysis of recorded instrument data.

Data Points: 2,000  
 Resolution: 1E-6 sec.  
 PCI: 2.0 mS  
 Peak-to-Peak Voltage: 2.20 kV  
 Joules per Pulse: 15.94  
 Pulses per Second: 14  
 Watts: 223.1  
 I<sub>RMS</sub> Amperes: 2.63  
 Frequency: 500 Hz

†† Only 1.20 mS shown

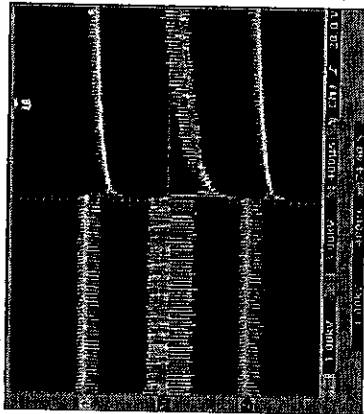


**Figure 19**  
Triple Trace, 16.14 Ohm Loading.

Three-trace screen capture. Channel 1 in yellow (top), Channel 2 in blue (bottom) and resulting differential, red trace (CHI - C2) in middle. Vertical scale settings for channels 1 & 2 and the differential trace are 1kV per division. Horizontal time scale setting is 400  $\mu$ S per division. Peak-to-Peak voltage is 2.54 kV. As in Figure No. 16, the PCI continues the form of a negative monophasic waveform.

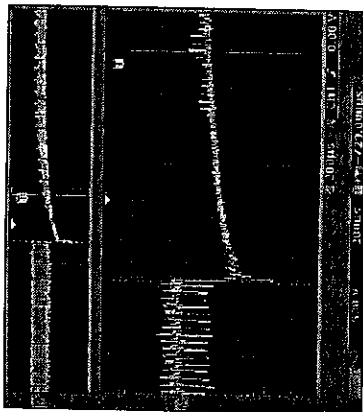


**Figure 20**  
Differential Trace at 16.14 Ohm Load. Waveform expansion.

Math trace of Figure 19. Vertical cursors zoom in on 1.2 mS segment of 2 mS PCI negative monophasic waveform.

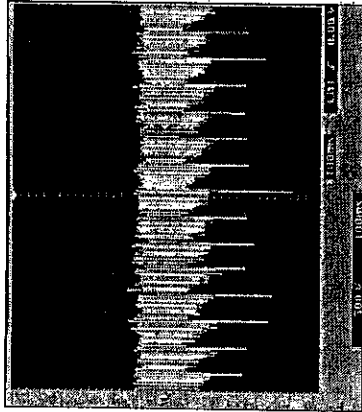


**Figure 22**  
Differential Trace at 16.14 Ohm Load at 100 mS/division.

Graph shows pulse repetition rate to be slightly more than 14 pulses or PCIs per second. Each negative peak represents a PCI impulse.

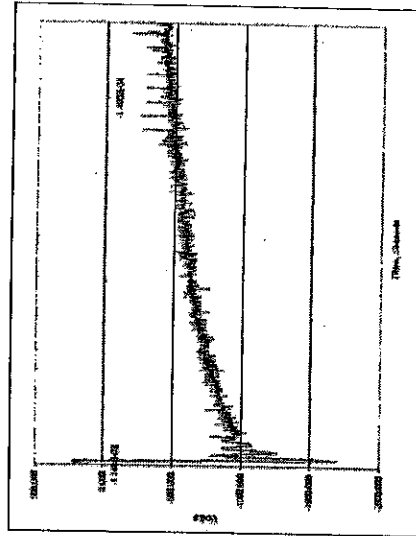


**Figure 21**  
16.14 Ohm Loading, 2.00 mS PCI (only 1.2 mS shown)

Waveform analysis of recorded instrument data.

- Data Points: 2,000
- Resolution, Seconds: 1E-6
- PCI: 2.0 mS
- Peak-to-Peak Voltage: 2.54 kV
- Joules per Pulse: 50.24
- Pulses per Second: 14
- Watts: 704.4
- I<sub>RMS</sub>, Amperes: 6.60
- Frequency: 500 Hz

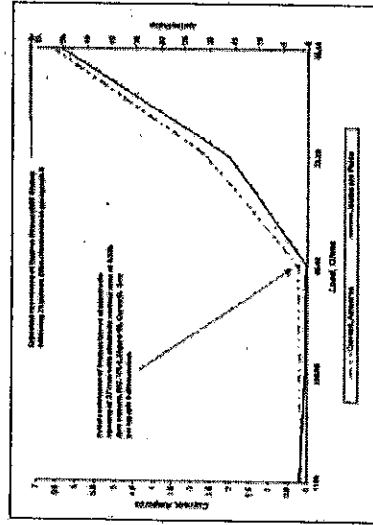


**Figure 23**  
Current and Joule Output as function of Load Resistance

This five-point plot describes energy output, both current and joule output as related to the five load experiments. The plot shows relatively constant current and Joule output until the load resistance reaches some point between 55 and 32 Ohms. At this knee-point, there is a steep rise in current and Joule output with decreasing resistance. Modeling with realistic resistance values approximating human tissue performance predicted for 37 mm spaced electrodes, we see that the current rapidly climbs to over 6.5 Amperes at 16 Ohms. As discussed in paragraph 6, when high voltage waveforms are applied to human tissue, resistance quickly falls within 20 pulses to a fraction of its initial value; therefore, the final predicted tissue resistance value is *off scale* in this graph.

## 8.0 Discussions

### 8.1 Frequency and Pulse Width

Taser International asserts that the energy output supplied by the weapon is different from the electrical energy provided by 60 Hz current, and refutes applicability of the reigning commercial-consensus industry standards governing electrical risk and safety: the IEC 479 series of standards. Taser asserts that these industry standards are inadequate in addressing the special high-frequency currents supplied by their product. However, Taser International does not propose an alternate industry standard, and instead offers findings from their own testing. Taser International's theory is that there is no electrical safety risk presented by their weapons to the heart and organs, because the current is too low, the pulse frequency is too high, and the pulse-width is too short.

The pulse spectrum bandwidth is evaluated over the portion of the pulse cycle having the maximum amplitude,<sup>49</sup> here, the fundamental component as represented by the first pulse cycle. As shown in Figures Nos. 7 through 15, at load resistances between 1100 Ohms and 55 Ohms, the frequency holds steadily although the PCI is observed to increase significantly with decreasing resistance. The pulse frequency bandwidth is simply the reciprocal of the pulse cycle, or in these cases  $1/20 \mu\text{s} = 50 \text{ kHz}$ . However, the tests show that the damped sinusoidal pulse continues and contributes substantive energy to the system for some time following the first pulse cycle. In Figure No. 15 we see system energy contribution continues for another  $50 \mu\text{s}$  before the waveform approaches zero; Figure Nos. 16 through 21 shows energy contribution for 2 mS, and so on. Despite this *extra* segment of significant energy being supplied to the human body by the Taser weapon, it has been omitted by the manufacturer. This omission is not trivial, since the analysis provided herein shows substantial energy contributions by these unaccounted segments. An analogy would be the incorrect accounting of the cargo tonnage of a freighter vessel by reporting only one of four fully loaded cargo holds.

Generally, we observe that the waveform energy contributing interval increases as the load resistance decreases. Using the test framework identified by the manufacturer (1000 Ohms +/- 10%), we notice a conflict with the pulse width claims made by Taser International since they report only a  $11 \mu\text{s}$  PCI when the tests performed herein show a 2 mS PCI. It is incorrect to analyze and predict risk to the human body by assuming and reporting only a fraction of the energy delivered.

### 8.2 Resistance

Because the Volt-Ampere-Resistance relationship is  $I = E/R$ , decreasing resistance must necessarily cause increasing current - *ceteris paribus*.

Nevertheless, the resistance value of 1000 Ohms used by the manufacturer in representing energy delivered by the weapon is unrealistically high and does not serve to model the energy delivered by the weapon in actual service. In tests performed by others on behalf of Taser, it appears this error is remarkably transitive, since these other researchers adopt the 1000-Ohm value without verification. Because of the  $I = E/R$  relationship, use of non-realistically high values of resistance in predictive computations of the weapon's performance serves to substantially understate the energy capable of being delivered by the weapon.

### 8.3 Independent Medical Testing Sponsored or Performed on Behalf of Taser International

In 1993 Robert Stratbucker reported on tests he performed on earlier stun-gun technology.<sup>50</sup> Stratbucker evaluated seven stun gun devices made by five manufacturers other than Taser International. Reporting on two devices loaded with a 20,000 Ohm dummy load, Stratbucker determined the output frequency to be 250 KHz for a  $4 \mu\text{s}$  pulse cycle in one unspecified model, and 500 KHz for a  $2 \mu\text{s}$  pulse cycle in another unspecified model (e.g., 1/pulse cycle). He did not report current delivered or any energy figure in any of these tests. In a later test involving a series of twelve experiments, Stratbucker tested the Air Taser Model No. 34000 using a pulse generator configured to simulate the electrical discharge performance of the handheld weapon. In this series of experiments, a 1000-Ohm load resistor bank was used to model tissue impedance. Resulting peak current values ranged from 8 to 18 Amperes, with reported pulse widths ranging from  $6.5 \mu\text{s}$  to  $13 \mu\text{s}$ , and intervals between pulses (i.e., dead space) ranging from 44 mS to 1000 mS. Because the units evaluated by Stratbucker provided considerably decreased output energy when compared to Taser models M18/ M26, Stratbucker's conclusions of product safety are not applicable to the Taser model M18/26 models. Additionally, the model resistance values used by Stratbucker are incorrectly too large, resulting in understated energy output values.

In the report prepared by Carlton University,<sup>51</sup> Harrison relied on the weapon electrical characteristics as supplied by Taser International, rather than instrument and verify such data himself. In this study, Harrison evaluated a pulse width of  $11 \mu\text{s}$  at a load of 1000 ohms - model values shown to be too high and resulting in radically understated energy output results.

Taser-commissioned tests performed by an Australian firm evaluated the Taser Model M26 using six nominal resistance values: 200, 300, 500, 1K, and 10K ohms.<sup>52</sup> No basis is provided for testing using the 10K Ohm resistance. Although the researchers tested the weapon in the drive-stun mode using the extended probes (i.e., distance between probes = 37 mm), the conclusions and comparisons made in the report are based on a 500 ohm model - an ohmic value that approximates roughly the contiguous distance from left-hand wrist to left

hand mid-thigh, a condition that has no realistic expectation for occurring in field deployment. As in the other Taser testing, the high resistance values used to compute energy, serves to substantively understate energy output values.

#### 8.4 Risks and Safety Findings

Let us consider the negative monophasic 2 ms, 2.2 kV peak-to-peak PCI discussed in Figure Nos. 16 through 18 generated with the 32.29 Ohm load resistor and evaluating to 2.63 Amperes rms body current. (Shock duration of a capacitor discharge<sup>†††</sup> =  $t_i > 1.8 \text{ ms}$ .) Applying the provisions of Chapter 6 of IEC 479-2 and evaluating this data against IEC 479-2 Figure 22 (*Threshold of Ventricular Fibrillation*) nomograph<sup>§§§</sup> maps to a region between risk curves  $C_2$  and  $C_3$  of Figure 22 - defining a region of risk residing between an average risk of fibrillation (up to 50% probability) and, a high risk of fibrillation (more than 50% probability). That is, in the drive-stun mode and without the air cartridge<sup>\*\*\*\*</sup> the Taser M18/M26 weapon placed on the body near the heart incurs a substantive risk for VF and death. This conclusion is conservative given the increasing current characteristic observed with decreasing resistance and the discussions herein regarding the dynamic resistance characteristic of biological tissue.

However, consideration of the electric current field patterns and current flow in tissue adjacent to the narrowly spaced electrodes must be made to evaluate risk when the weapon is applied to other body areas. Fish and Geddes<sup>§§</sup> noted that current flows from one power-source terminal to the other along multiple nearly-parallel 3-D paths, and that unless there is just one type of tissue, the current does not all flow through a path of least resistance, as is sometimes claimed. Fish and Geddes noted that the current flow pattern is dependant upon the conductivities of the various tissue and their arrangements, and that application of large voltages can stimulate excitable cells of surrounding tissue. Reilly also concluded that notions of body current flowing in a path of least resistance between two electrodes were wrong.<sup>§§</sup> Figure 24 below delineates the field lines for a typical dipole system representative of the 37 mm spaced integral electrodes on the Taser M18/26 weapons - showing multiple and wide current flow paths between weapon electrodes, and not a flow in a narrow, direct, straight

††† Shock-duration of a capacitor discharge ( $t_p$ ): The time interval from the beginning of the discharge to the time when the discharge current has fallen to 5% of its peak value (IEC 479-2, Clause 3.4)

§§§ Fibrillation risks for current flowing in the path hand to feet.

\*\*\*\* The air cartridge introduces losses as discussed in Figure No. 5 herein. It is expected that the current supplied at the extended terminals of the air cartridge would likely evaluate to lower current levels than measured for the integral electrodes because of inherent system losses; however, the current supplied at the terminals of the air cartridge is not evaluated in this paper.

line path between electrodes. Although the IEC 479-1 Figure 22 risks for VF are greatest when the weapon electrodes are placed to the chest or back within the proximity of the heart, it is evident that substantive VF risk is still at hand when the heart area and electrodes are spaced by some distance, although reducing with greater spacing. However, because of the great amount of current and long pulse duration, electrode placement anywhere on the torso within one foot of the heart area supplies a significant VF risk, as well as a risk for respiratory arrest. Reilly also produced data resulting from experiments with dogs showing that the ventricular fibrillation threshold occurs at a peak current of 15 mA +/- 4.3 mA for single DC pulse of 1 ms duration.<sup>§§</sup> Therefore, the energy (6.6 Amperes @ 2 mS) supplied by the Taser weapon can easily be understood to incur a substantive risk of injury and/or death.

It is important to note that the provisions of the IEC 479-2 standard<sup>§§</sup> only evaluate VF risk for a single pulse, and not 14 pulses per second as supplied by the Taser M18 weapon with a fresh set of batteries, since repetitive pulses are far more dangerous than a single pulse. Reilly notes, as does Bernstein, that oscillatory stimuli can significantly enhance the biological response that might otherwise result from a single pulse, and that the fibrillation threshold falls steadily with the increasing number of pulses. Bernstein emphasizes the importance of pulse repetition in electric safety and states that the hazard in the output would be increased if the pulse repetition rate should increase or the amplitude of the output increased.<sup>§§</sup> In fact, Reilly shows the VF threshold to fall by a factor of thirty with a train of six 1 mS pulses.<sup>§§</sup> Geddes also finds VF to be more easily induced by rapidly occurring stimuli. Geddes concludes, "when the repetition frequency exceeds five stimuli per second, the human ventricles are reaching the limit of their ability to respond to each stimulus, and the stimuli fall in the vulnerable period of the previous beat and the risk of fibrillation is high if the stimulus intensity is suprathreshold."<sup>§§</sup> Therefore, rapidly repeating pulses supplied by the Taser M18/26 weapons create a greater risk for VF than the single pulse framework covered in IEC 479-2 Figure 22.

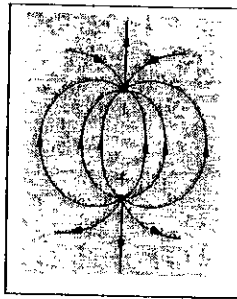


Figure 24

Typical dipole system field lines showing typical current flow in human tissue. An electric dipole consists of two charges of equal and opposite sign ( $-q, +q$ ), separated by distance  $L$ . The electric dipole moment is the product  $p=qL$ , which measures the strength of the dipole.

Also, the IEC 479 series of standards only addresses VF risk to healthy hearts, and does not assess VF risk in myopathic (diseased) hearts. According to Lucy<sup>§§</sup> and Kavanagh<sup>§§</sup>, the myopathic heart is considerably more vulnerable; they determined a four-fold difference in the defibrillation threshold for the diseased heart when contrasted to a healthy heart. Ford and Geddes report precipitation

1222

of VF during the heart's vulnerable period in a heart altered to simulate cardiomyopathy and using a static electricity discharge common in the household by walking on the carpet, combing hair, or removing clothing.<sup>62, 63</sup> Similarly, McCarty and Glasser also determined a definite connection for static electricity induced VF in a dog with a diseased heart.<sup>64</sup> Consequently, the myopathic heart is more susceptible to VF and the effects of electric shock, including the extremely low-level currents inherent in everyday household static electricity.

### 9.0 Conclusions

The manufacturer's design for a high, unloaded spark-gap voltage of 50 kV appears to be based upon the breaking down the six series air-gaps connections (described in Figure No. 5) while in the ballistic mode of operation. That is, the basis for 50 kV output has more to do with the method of conveying energy and inherent losses in the system from the weapon to the target, given the air-gap electrical connection architecture, and less to do with issues relating to subject incapacitation. The weapon also does not provide regulating means to limit or control output energy when in the drive-stun mode versus the ballistic mode. The design losses considered while the weapon is in the ballistic mode of operation are not present in the drive-stun mode, and thus the weapon is capable of supplying considerably more energy in the drive-stun mode than in the ballistic mode. This increase of delivered energy capacity in the drive-stun mode is not reflected in the manufacturer's specifications, particularly when considering realistic tissue resistance values. The need for such high voltages, and thus more overall energy, could have been easily eliminated had the manufacturer selected a direct electrical connection method for all contact points between the weapon and electrode bars, in lieu of the spark gap or insulation breakdown method.

The PCI reported by the manufacturer, 11  $\mu$ S at a 1000-Ohm loading is about 200 times less than the actual measured PCI value of 2 mS. This deficiency is important in that most of the energy supplied by the weapon is unaccounted, particularly when evaluating realistic human tissue resistances corresponding to the 37 mm spacing between electrodes. As shown herein, decreasing load resistance causes increasing PCI, resulting in increased overall current and Joule output, and therefore increasing the risk of VF, damage to organs and tissue, and death.

With the Taser M18/M26's pulse repetition frequency of 14/20 pulses per second, it is appropriate to apply Gowrishankar's findings regarding rapidly reduced resistance following application of the high-voltage pulses. Given the test findings from the Taser M18 in the stun-gun mode of operation and using realistic human tissue resistance values, we can conclude the Taser M18/M26 can be lethal when used in the drive-stun mode of operation and can kill when contrasted to the reference criteria contained in commercial consensus standards and in other scholarly publications.

### References

1. Report from Robert G. Harrison of Carleton University, Ottawa, Canada, to, Stephen D. Tuttle of Taser International, Inc., dated 14 February 2000.
2. Advanced Taser, M-Series Operating Manual, Models M26-Model 44000, M19L- Model 44001, M18 - Model 44002 (packaged with the actual M18L device tested in this paper)
3. Harrison op.cit.
4. Aleksandrov, N.L., Bazelyan, E.M. "Ionization processes in spark discharge plasmas" 1999 Plasma Sources Sci. Technol. 8 285-294
5. IEEE Std 1584-2002, "IEEE Guide for Performing Arc-Flash Hazard Calculations." IEEE Press, Piscataway, New Jersey.
6. Institute of Electrical and Electronic Engineers, (IEEE), IEEE Std. C37.90.1-2002, "IEEE Standard for Surge Withstand Capability (SWC) Tests for Relays and Relay Systems Associated with Electric Power Apparatus." IEEE Press, Piscataway, New Jersey.
7. International Electrotechnical Commission (IEC) IEC 60255-22-4 (2002-04), "Electrical Relays-Part 22, Electrical Disturbance Tests for Measuring Relays and Protection Equipment- Electrical Fast Transient/Burst Immunity Test," International Electrotechnical Commission (IEC), Brussels, Belgium.
8. International Electrotechnical Commission (IEC) IEC 60255-22-1 (2002), "Electrical Disturbance Tests for Measuring Relays and Protection Equipment-Section 1: 1 MHz Burst Disturbance Tests," IEC, Brussels, Belgium.
9. Institute of Electrical and Electronic Engineers, (IEEE), IEEE STD 100-1996, The IEEE Standard Dictionary of Electrical and Electronics Terms, 6th edition.
10. Institute of Electrical and Electronic Engineers, (IEEE) IEEE Std. 4-1995, IEEE Standard Techniques for High-Voltage Testing
11. Bowdler, G.W. (1973) "Measurements in high-voltage test circuits." 1st edition. New York City, NY. Pergamon Press Inc.
12. Park, J. H. and Cones, H. N., "Spark-Gap Flashover Measurements for Steeply Rising Voltage Impulses," Journal of Research of the National Bureau of Standards, Section C (Engineering and Instrumentation), Vol. 66c, No. 3, pp. 197-207, July/Sept. 1962.
13. International Electrotechnical Commission (IEC) 60469-1, Pulse techniques and apparatus, Part 1: Pulse terms and definitions, 2nd edition, 1987-12

14. International Electrotechnical Commission (IEC) 60469-2, Pulse techniques and apparatus, Part 2: Pulse measurement and analysis, general considerations, 2nd edition, 1987-12
15. Institute of Electrical and Electronic Engineers, (IEEE) IEEE Std. 181-2003 Standard on Transitions, Pulses and Related Waveforms.
16. International Electrotechnical Commission (IEC) 61000-4-4, Electromagnetic compatibility (EMC), Part 4-4: Testing and measurement techniques - Electrical fast transient/burst immunity test, 2nd edition, 2004-7
17. Tektronix technical brief: 1998. "Floating Oscilloscope Measurement and Operator Protection." Tektronix, Inc. Beaverton, Oregon.
18. White, R.A. (2002) "Electronic Test Instruments: Analog and Digital Measurements", 2nd edition. New York City, NY. Prentice Hall
19. Kularatna, N. "Modern Electronic Test and Measuring Instruments." 2005. UK, Institute of Electrical Engineers (IEE) Press.
20. Kind, D., Feser, K. (2000) "High Voltage Test Techniques." Woburn, MA. Newnes Press.
21. Fish, Raymond, Geddes, Leslie (2003) "Medical and Bioengineering Aspects of Electrical Injuries" Lawyers & Judges Publishing Co. Tucson, AZ. Chapter 11.6, Pg. 103
22. O'Neil, Peter V. (1983) "Advanced Engineering Mathematics," Third edition. Belmont, CA. Wadsworth Publishing Co.
23. *ibid.*
24. *ibid.*
25. Letter from Dr. Theodore Bernstein, University of Wisconsin, Madison to Mr. Neil Zyllich, Consumer Product Safety Commission, dated 12 February, 1976
26. International Electrotechnical Commission (IEC) IEC 479-1, "Effects of Current on Human Beings and Livestock, Part 1, General Aspects, 1994-09" (Figure 2) Table 2 and Figure 4
27. *ibid.* Figure 2 Table 3, Test Series A, and Clause 2.5.1
28. *ibid.* Figure 2
29. Fish, Geddes *op.cit.*, Chapter 1.1, Pg. 105, and Chapter 24.5, Pgs. 255/256
30. Gowrishanker, T.R., Piquett, UWE, Weaver, James C., 1999, Changes in Skin Structure and Electrical Properties following High Voltage Exposure. Annals of the New York Academy of Science., 888: 883-194 (1999)

31. Reilly, J.P. (1998). Applied Bioelectricity, From Electrical Stimulation to Electropathology, chapter 10.2, page 415. Springer
32. Brian James Daley, MD, et al "Electrical Injuries" Medline, Nov 17, 2004.
33. Prausnitz, M.R., V.G. Bose, R.Langer & J.C. Weaver, 1993. Electroporation of mammalian skin: a mechanism to enhance transdermal drug delivery. Proceedings of the National Academy of Science. U.S.A. 90:10504-10508.
34. Gowrishanker *op.cit.*
35. Gunderson M., Vernier T., et al (2002) "Ultrasound-Pulsed Electroporation: Applications of High Pulses Electric Fields to Induce Caspase Activation of Human Lymphocytes," Proc. IEEE High Voltage Workshop, July, 2002, pp. 667-671.
36. Schoenbach HS, Beebe S.J., Buescher E.S., "Intracellular Effect of Ultrasound Pulses," J. Bioelectromagnetics, Vol 22, September, 2001, pp.440-448.
37. Reilly *op.cit.*, Chapter 7.5, Pg. 265.
38. Reilly *op.cit.* Chapter 7.5, Pg. 269.
39. Koscove, Eric M. The Taser Weapon: A New Emergency Medicine Problem, Annals of Emergency Medicine. December 1985
40. IEC 479-1, *op.cit.* Clause 5.3
41. *ibid.* Clause 6.3
42. Geddes, L.A., et al The mechanism underlying sudden death from electric shock, Medical Instrumentation, Vol. 20, No. 6, Nov-Dec 1986
43. Fish, Raymond, Geddes, *op.cit.* Pg 201.
44. Fish, Raymond, Geddes, *op.cit.* Pg 202.
45. Ruggieri, James A. American Academy of Forensic Science (AAFS) abstract proceedings "Lethality of Tasers" February 25, 2005 New Orleans.
46. Reilly *op.cit.* Chapter 7.5, Pg. 268.
47. IEC 479-1, *op.cit.* Clause 2.5.4, Figure 9
48. Reference Data for Radio Engineers, (1977) ITT/Howard W. Sams & Co. 6th Edition.
49. IEEE 100 *op.cit.*
50. Stratbucker, R.A. (1993) The relative immunity of the skin and cardiovascular system to the direct effects of high voltage- high frequency components electrical pulses. 1993, IEEE Press

51. Harrison op.cit.
52. Advanced Taser M-26 Safety Analysis, Biomedical Engineering, The Alfred, dated 22 September 2003
53. Fish, Raymond, Geddes, op.cit. Pg 106
54. Reilly op.cit. Chapter 10.2, Pg 415.
55. Ibid. Table 6.4, Pg. 209.
56. International Electrotechnical Commission (IEC) IEC 479-2, "Effects of current passing through the human body, Part 2, Special Aspects, Second edition, 1987
57. Analysis of Dr. Theodore Bernstein to CPSC BES, dated 12 February, 1976.
58. Reilly op.cit. Figure 6.6, Pg. 208.
59. Fish, Raymond, Geddes op.cit. Chapter 18, Pg. 198
60. Lucy, S.D., Jones, D.L., and Klein, G.J. 1994. Pronounced increase in defibrillation threshold associated with pacing-induced cardiomyopathy in the dog. *American Heart Journal*. 127: 366-376
61. Kavanagh, K.M., Guerrero, P.A., Jugdurt, B.I, Witkowski, F.X. Saffitz, J.E. 1999. Electrophysiologic properties and ventricular fibrillation in normal and myopathic hearts. *Can. J. Physiol. Pharmacol.* 77:510-519
62. Ford, G.L., Geddes, L.A., Transient ground-potential rise in gas insulated substations - assessment of shock hazard. *IEEE Trans. Power App. Sys.* 1982; PAS-101 (10): 3620-9
63. Fish, Raymond, Geddes op. cit. Chapter 12, Pg. 117, and Chapter 38, Pgs. 385, 389
64. McCarty, R.J., Glasser, S.P. The arrhythmogenic effect of static electricity on the dog heart. *American Heart Journal*. 1977;93:496-500